Stick-Slip Control in Nanoscale Boundary Lubrication by Surface Wettability

Wei Chen[1,2], Adam S. Foster[1], Mikko J. Alava[1], and Lasse Laurson[1*]
[1] *COMP Centre of Excellence, Department of Applied Physics, Aalto University, P.O. Box 11100, 00076 Aalto, Espoo, Finland and*
[2] *Supercomputing Center of CAS, Computer Network Information Center, Chinese Academy of Sciences, Beijing 100190, China*

We study the effect of atomic scale surface-lubricant interactions on nanoscale boundary-lubricated friction, by considering two example surfaces - hydrophilic mica and hydrophobic graphene - confining thin layers of water in molecular dynamics simulations. We observe stick-slip dynamics for thin water films confined by mica sheets, involving periodic breaking-reforming transitions of atomic scale capillary water bridges formed around the potassium ions of mica. However, only smooth sliding without stick-slip events is observed for water confined by graphene, as well as for thicker water layers confined by mica. Thus, our results illustrate how atomic scale details affect the wettability of the confining surfaces, and consequently control the presence or absence of stick-slip dynamics in nanoscale friction.

PACS numbers: 62.20.Qp, 68.35.Af, 68.08.Bc

Understanding friction plays a central role in technological applications and phenomena in diverse fields ranging from micromechanical devices to bioengineering [1] and to earthquakes [2]. Given the continuing miniaturization of mechanical devices towards the nanoscale [3], improved understanding of friction and wear could help in reducing energy consumption, improving reliability and extending service life. Indeed, an important part of their design process consists of trying to minimize friction and to eliminate stick-slip dynamics [4].

Stick-slip control in lubricated friction is of particular importance given the vast amount of applications where lubricants are used to reduce the detrimental effects of friction and wear [5]. Examples of mechanisms behind the emergence of stick-slip in boundary-lubricated systems have been numerically demonstrated to include repeated crystallization and shear melting of the thin lubricant film [6], interlayer slips within the ordered solid-like lubricant film, or wall slips at the wall-film interface [7]. Most of the numerical studies of stick-slip in boundary lubrication have focused on coarse-grained or simplified/idealized models [6, 8, 9], not explicitly considering the atomic scale interactions occurring in real systems. On a coarse-grained scale, a useful classification of the lubricant-surface interactions is given by the wettability of the confining surfaces by the lubricant, with systems displaying a larger contact angle/lower wetting generally exhibiting lower friction. Other approaches to friction control include e.g. applying mechanical oscillations [10, 11]. While the effect of wettability on lubricated friction has been studied experimentally in macroscopic [12–15] and nanoscale [16] systems, and modeled using phenomenological finite-element models [17] and simplified molecular dynamics (MD) simulations of nanopatterned surfaces [18, 19], less is known about the underlying atomic scale processes and mechanisms responsible for the presence or absence of stick-slip.

Given the large surface-to-volume ratio in boundary lubrication, nature of the interaction between the lubricant and the confining surfaces originating from their atomic composition should play a crucial role. Thus, we study the interaction of a thin water layer (thickness h around 0.5 nm unless stated otherwise) in MD simulations using full atomic models of two experimentally relevant confining surfaces with different wetting characteristics: crystalline mica, a hydrophilic substrate that strongly adsorbs water [20] and graphene, a hydrophobic surface interacting weakly with water [21], see Fig. 1. We ob-

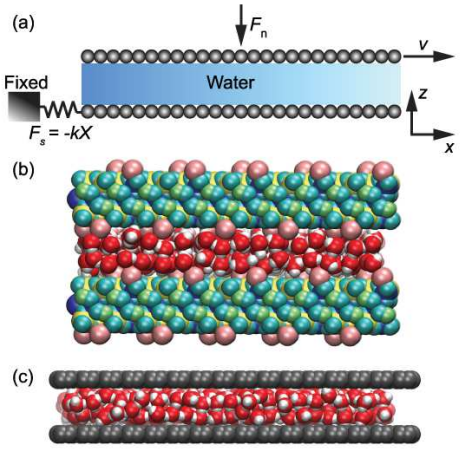

FIG. 1. (color online) (**a**) The geometry of the simulation system. Solid sheets are held together by a constant normal load F_n. The top sheet is moving at a constant velocity V, and the bottom sheet is connected to a fixed stage by a spring of stiffness k. The water molecules are confined by (**b**) two mica sheets (each of thickness of 8.34 Å) or (**c**) two monolayer graphene sheets. The color code of the atoms is: water oxygen (red), water hydrogen (white), potassium (pink), silicon (yellow), aluminum (blue), mica oxygen (cyan), mica hydrogen (lime), and carbon (gray).

serve stick-slip dynamics for thin water layers confined by mica: each unit cell of mica contains two K^+ ions, interacting strongly with the water oxygens via Coulomb interactions, leading to formation of atomic scale capillary bridges next to the K^+ ions, connecting the two mica surfaces in the stick state. These bridges break during the subsequent slip event, and reform during the next stick phase, a process that is also visible as the breaking and reforming of interfacial hydrogen bonds between water and mica. This mechanism is different from both the crystallization-shear melting transitions [6] and interlayer or lubricant-surface slips [7] observed before in simplified models. In contrast, water films confined by hydrophobic graphene, as well as thicker water layers confined by mica, exhibit fundamentally different dynamics with no stick-slip.

To model the confined water film, we consider systems ranging from 200 to 1200 SPC/Fw water molecules [22]. We consider 2M1-muscovite mica with the formula $KAl_2(Al, Si_3)O_{10}(OH)_2$, with the force field parameters from Ref. [23]. One mica surface consists of 10×6 unit cells, and has linear dimensions of $L_x = 52.07$ Å and $L_y = 54.036$ Å, see Fig. 1. To create site disorder, mimicking a real mica surface with a random distribution of potassium ions on it, one K^+ ion of the pair in each unit cell is removed and subsequently placed on the bottom part of the sheet [24]. The graphene sheets have $L_x = 68.063$ Å and $L_y = 36.841$ Å. The Lennard-Jones parameters for carbon are from Ref. [25]. The cutoff radius is $r_c = 10.0$ Å for all potentials. Both sheets are parallel to the xy plane with periodic boundary conditions along the x and y directions. Couette flow is generated by moving the top sheet at a constant velocity V along the x direction. The distance between parallel sheets is allowed to vary, and a constant normal load $F_{\rm n}$, giving rise to a pressure $P_\perp$, is applied on the top sheet. The bottom sheet is constrained to move along the x axis, and is attached to a spring of stiffness $k/N_{\rm p} = 0.0035$ N/m, where $N_{\rm p}$ is the total number of atoms in a sheet. The other end of the spring is connected to a fixed stage. Temperature of $T = 295$ K is maintained using a Langevin thermostat, applied only in the y direction to avoid streaming bias [26, 27]. The equations of motion are solved with the velocity Verlet algorithm implemented in the LAMMPS code [28], with an integration time step of 1 fs. Long-range electrostatic interactions are computed using the particle-particle particle-mesh (PPPM) solver with 10^{-5} accuracy. Initially the water molecules are arranged in a simple cubic lattice. The simulations are first run for 100 ps with both surfaces kept fixed, followed by 100 ps during which the top surface is subject to a normal force $F_{\rm n}$ and is allowed to move vertically. Then, the top surface is driven horizontally with a velocity V for 1 ns to generate the steady state, after which we continue the simulations for approximately 60 ns, recording the observables of interest.

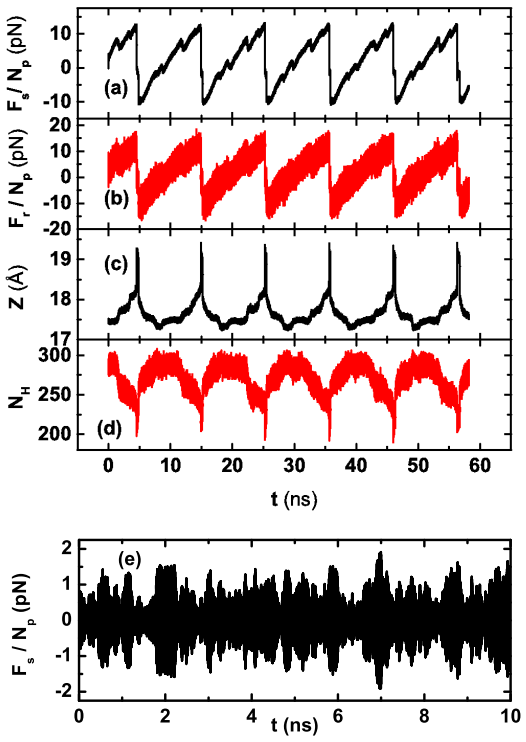

FIG. 2. (color online) Time evolution of (**a**) the spring force per sheet atom, (**b**) the friction force per sheet atom on the bottom mica sheet applied by the water and the top mica sheet, (**c**) the position Z of the center of mass of the top mica sheet in the z direction, and (**d**) the number of hydrogen bonds between the 256 mica-confined water molecules and the bottom mica sheet. (**e**) Spring force per sheet atom for 200 water molecules confined by graphene sheets. $V = 0.1$ m/s and $P_\perp = 1$ atm in both cases.

Simulation results for 256 water molecules confined by mica sheets for $P_\perp = 1$ atm and $V = 0.1$ m/s are shown in Fig. 2. The force per atom on the bottom sheet applied by the spring, $F_{\rm s}/N_{\rm p}$, exhibits characteristic stick-slip behavior [Fig. 2 (a)]. Fig. 2 (b) shows the friction force per sheet atom on the bottom mica plate applied by the water and the top mica plate, $F_{\rm r}/N_{\rm p}$, exhibiting similar time-dependence as the spring force, with superimposed high-frequency fluctuations due to the finite temperature. Fig. 2 (c) shows the position Z of the center of mass of the top sheet in the z direction. The center of the bottom mica sheet is fixed at $z = 4.16$ Å. During each slip event, Z increases by roughly 10% [6]. Since formation and breaking of interfacial chemical bonds is known to play a role in friction (see Ref. [29] for an example from rock friction), we show also the time-dependence of the number of hydrogen bonds (i.e. the number of water hydrogens closer than 3 Å from the bottom mica surface) between water and the bottom mica surface in Fig. 2 (d): bonds break as the system evolves from stick to the slip state.

For comparison, we also performed MD simulations of

water confined by hydrophobic graphene sheets. We varied the number of water molecules from 200 to 1200, the normal loads from $P_\perp = 1$ to 10 atm, and the driving velocities from $V = 0.01$ to 0.1 m/s. Fig. 2 (e) shows the spring force from simulations of 200 water molecules, $P_\perp = 1$ atm, and $V = 0.1$ m/s; similar results are obtained for other $P_\perp$ and V values. We observe a small increase of friction with V for both mica and graphene, see Supplemental Material [30], and Refs. [31, 32] for experimental results on mica-confined systems with sliding velocities significantly lower than those reachable in our MD simulations. Our simulations thus demonstrate that the stick-slip behavior does not arise for thin water films confined by graphene. Instead, continuous, smooth sliding with the maximum friction force well below that obtained for mica is observed for all parameter values considered. We also note that the same applies to the mixed system with one graphene and one mica surface: slip is localized at the hydrophobic graphene-water interface, and no stick-slip is observed.

This difference between the two kinds of surfaces may be explained by the relatively strong interaction of the potassium ions on the mica surfaces with the oxygen atoms of the water molecules via Coulomb interactions. Thus, the ions could act as "freezing nuclei", with the water molecules gathering around them to form nanoscale capillary water bridges [33, 34], connecting the top and bottom surfaces within the stick phase. As the system starts to slip, these bridges would break. The interaction of carbon atoms with oxygen is much weaker, and we expect that no capillary bridges are formed between graphene sheets, explaining the absence of stick-slip dynamics in that case.

To verify this hypothesis, we calculate the density distributions $\rho(x, y)$ of water oxygens in the contact layer relative to the bottom surfaces. Fig. 3 (a) shows $\rho(x, y)$ for a water film confined by mica sheets when the system sticks [$t = 1$ ns in Fig. 2 (a)]. Peaks in $\rho(x, y)$ are located at the K^+ ions. Fig. 3 (b) presents the corresponding $\rho(x, y)$ during the first slip state when $t = 5$ ns [cf. again Fig. 2 (a)]: the peaks of $\rho(x, y)$ become smaller and broader. Finally, Fig. 3 (c) shows $\rho(x, y)$ for the subsequent stick state at $t = 7$ ns [Fig. 2 (a)], where we again observe that the peaks are as high and narrow as those of the previous stick state.

To gain more insight into the nucleation and breaking of the capillary bridges between the surfaces, we calculate the density profiles $\rho(z)$ of water oxygens across the gap. When the system is slipping [Fig. 3 (d)], $\rho(z)$ exhibits two separate peaks, consistent with breaking of the capillary bridges. In the stick state [Fig. 3 (e)], $\rho(z)$ exhibits multiple peaks spanning the gap. This can be understood as the water molecules forming nanoscale capillary bridges between the two mica surfaces. In contrast to this behavior, the density distributions $\rho(x, y)$ of the water film consisting of 200 water molecules confined

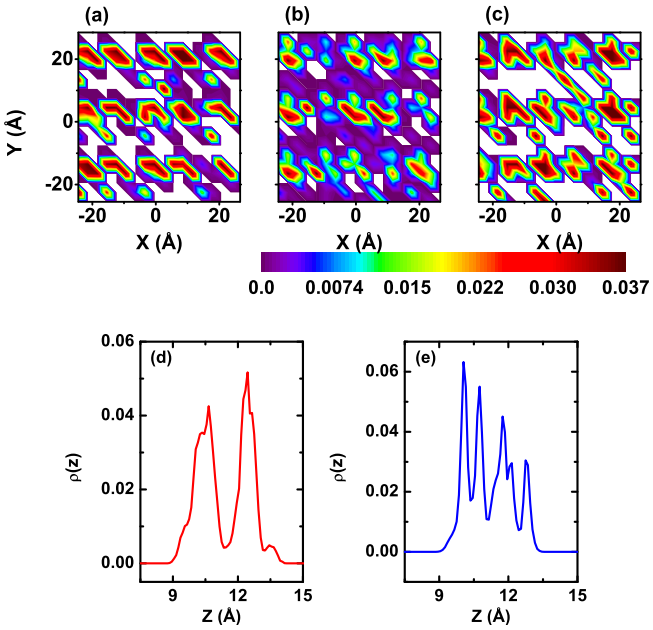

FIG. 3. (color online) Contour graphs of the density distribution $\rho(x, y)$ of water oxygens in the contact layer relative to the bottom mica surface for (**a**) $t = 1$ ns ("stick"), (**b**) $t = 5$ ns ("slip"), and (**c**) $t = 7$ ns ("stick"). White corresponds to no water molecules being present. The density profiles across the gap, $\rho(z)$, of water confined by mica sheets when the system (**d**) slips and (**e**) is in the stick state. In both (**d**) and (**e**), the top surface of the bottom mica sheet is at $z = 8.3$ Å, while the lower surface of the top mica sheet is at $z = 14.7$ Å in (**d**) and at $z = 13.4$ Å in (**e**).

by graphene sheets in Fig. 4 show that water clusters to form a single, relatively large droplet-like structure between the two graphene sheets, without any apparent signature of breaking-reforming transitions. The corresponding density profiles $\rho(z)$ [30] are similar to previous observations in equilibrium graphene-confined systems [35].

Thus, when the two mica surfaces are very close together, the thin confined water film loses its fluidity, and the bulk flow properties of water play little or no role in friction. However, they may be recovered by increasing the thickness of the water layer [36], with the conditions approaching those of hydrodynamic lubrication. To this end, we performed MD simulations with four different, larger thicknesses of the water layer: $h = 1.77$, 2.03, 2.29, and 2.56 nm, corresponding to 1536, 1792, 2048, and 2304 water molecules, respectively. For these thicker water films, the stick-slip dynamics disappears. Instead, smooth sliding dynamics is observed, which at a first glance looks similar to that in the graphene-confined system. However, subtle differences can still be observed between the two surfaces. Zooming in to the spring force time series (e.g. the one shown in Fig. 2(e)] reveals periodic oscillations corresponding to the eigenfre-

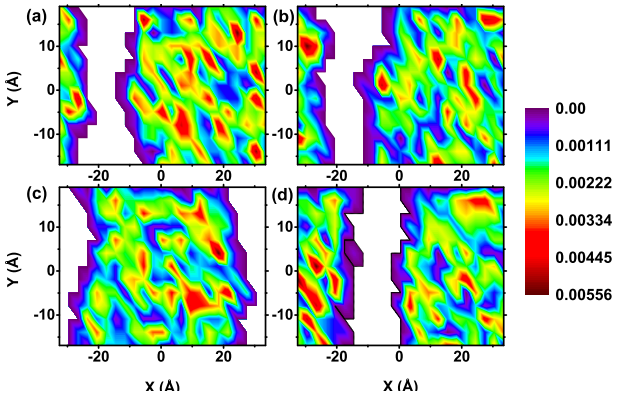

FIG. 4. (color online) Contour graphs of the density distribution $\rho(x, y)$ of water oxygens in the contact layer relative to the bottom graphene surface for (**a**) $t = 0$ ns, (**b**) $t = 3$ ns, (**c**) $t = 5$ ns and (**c**) $t = 8$ ns. White corresponds to no water molecules being present.

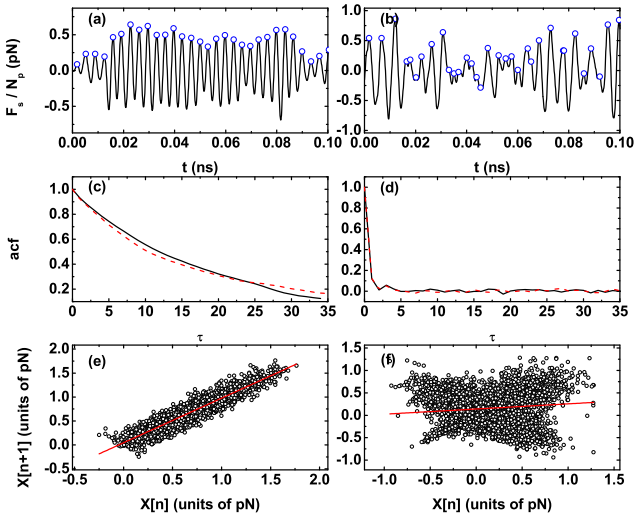

FIG. 5. (color online) Time dependence of F_s/N_p during a time period of 0.1 ns (**a**) for 1200 graphene-confined and (**b**) for 1536 mica-confined water molecules. Blue circles show the local maxima of the signals, corresponding to the time-varying amplitudes $X(n)$ of the spring force oscillations. The autocorrelation functions (as a function of the lag $\tau \equiv n - n'$) of these amplitudes are given (**c**) for graphene and (**d**) for mica, extracted from 10 ns long spring force signals. The solid lines correspond to the simulation results, while the dashed lines show the corresponding ACFs from the autoregressive model. The plots of $X[n+1]$ vs $X[n]$ extracted from the simulations for (**e**) graphene and (**f**) mica further illustrate the different nature of the smooth sliding dynamics for the two kinds of confining surfaces. The slopes of the lines (linear fits) are 0.9 and 0.1 for graphene and mica, respectively.

quencies of the spring-bottom plate mass (M) system, $f = 1/(2\pi)\sqrt{k/M}$. For both surfaces, the varying amplitudes of these oscillations at each period [blue circles in Figs. 5(a) and (b)] form sequences of time-ordered observations $X(n)$ which can be well-described by an autoregressive model $X(n+1) = \alpha X(n) + W(n)$ [or equivalently, the Ornstein-Uhlenbeck process $X(n+1) - X(n) = -(1-\alpha)X(n) + W$], with W white noise originating from the interaction with the fluctuating lubricant and α a model parameter, both extracted using the R package [37]. For water confined by graphene, we find $\alpha \approx 0.8$ and $\delta W \approx 0.1$ pN for all conditions considered, while we find $\alpha \approx 0.1$ and $\delta W \approx 0.3$ pN for thick water films ($h \geq 1.77$ nm) confined by mica. Accordingly, the autocorrelation function (ACF) of $X(n)$ for mica decays more rapidly to zero than its counterpart for graphene. In both cases the ACFs computed from the simulation data agree with those of the corresponding autoregressive model [see Figs. 5 (c) and (d)]. The observation that δW does not significantly depend on h for $h \geq 1.77$ nm indicates that the screened mica-water interaction has a sub-nanometer range, resulting essentially in a surface effect of the fluctuations of the water layer. Also, the stronger interaction of mica with the fluctuating lubricant (as compared to that of graphene) results in a factor of three larger δW [see also Figs. 5 (e) and (f)].

In summary, the presence or absence of breaking-reforming transitions of local capillary bridges in the water film, controlled by the atomic structure and the ensuing wettability (hydrophilic mica vs hydrophobic graphene) of the confining surfaces, plays a crucial role in whether stick-slip dynamics is observed or not. For mica, the decisive role of the K^+ ions in the formation of the nanoscale capillary bridges suggest that the microscopic details behind stick-slip dynamics should in general depend on the atomic structure of the system, and it would be interesting to perform similar studies for other confining surfaces with different surface-lubricant interactions. Nevertheless, we expect our main observations to be rather general, and to open up interesting possibilities in controlling nanoscale boundary-lubricated friction by tuning the wettability of the confining surfaces.

We acknowledge the financial support by the Academy of Finland through the Centres of Excellence Program (project no. 251748) and via an Academy Research Fellowship (L.L., project no. 268302). We are also grateful to the COST action MP1303. The calculations presented above were performed using computer resources within the Aalto University School of Science "Science-IT" project. We also acknowledge the computational resources provided by CSC (Finland).

* lasse.laurson@aalto.fi

[1] C. Majidi, R. E. Groff, Y. Maeno, B. Schubert, S. Baek, B. Bush, R. Maboudian, N. Gravish, M. Wilkinson, K. Autumn, and R. S. Fearing, Phys. Rev. Lett. **97**, 076103 (2006).
[2] C. H. Scholz, Nature **391**, 37 (1998).

[3] B. Bhushan, J. N. Israelachvili, and U. Landman, Nature **374**, 607 (1995).
[4] J. H. Dieterich, Pure Appl. Geophys. **116**, 790 (1978).
[5] B. J. Hamrock, S. R. Schmid, and B. O. Jacobson, *Fundamentals of fluid film lubrication*, Vol. 169 (CRC press, 2004).
[6] P. A. Thompson and M. O. Robbins, Science **250**, 792 (1990).
[7] Y. Lei and Y. Leng, Phys. Rev. Lett. **107**, 147801 (2011).
[8] W. Chen, S. Kulju, A. Foster, M. Alava, and L. Laurson, Phys. Rev. E **90**, 012404 (2014).
[9] A. Jabbarzadeh, P. Harrowell, and R. I. Tanner, Phys. Rev. Lett. **96**, 206102 (2006).
[10] R. Capozza, A. Vanossi, A. Vezzani, and S. Zapperi, Phys. Rev. Lett. **103**, 085502 (2009).
[11] F. Giacco, E. Lippiello, and M. P. Ciamarra, Phys. Rev. E **86**, 016110 (2012).
[12] Z. Pawlak, W. Urbaniak, and A. Oloyede, Wear **271**, 1745 (2011).
[13] B. Bhushan and Y. C. Jung, J. Phys.: Condens. Matter **20**, 225010 (2008).
[14] M. Kalin and M. Polajnar, Tribol. Lett. **52**, 185 (2013).
[15] A. Borruto, G. Crivellone, and F. Marani, Wear **222**, 57 (1998).
[16] K. Mougin, G. Castelein, and H. Haidara, Tribol. Lett. **17**, 11 (2004).
[17] L. Joly and T. Biben, Soft Matter **5**, 2549 (2009).
[18] C. Cottin-Bizonne, J.-L. Barrat, L. Bocquet, and E. Charlaix, Nature Mater. **2**, 237 (2003).
[19] R. Capozza, A. Fasolino, M. Ferrario, and A. Vanossi, Phys. Rev. B **77**, 235432 (2008).
[20] Y. Leng and P. T. Cummings, J. Chem. Phys. **124**, 074711 (2006).
[21] O. Leenaerts, B. Partoens, and F. Peeters, Phys. Rev. B **79**, 235440 (2009).
[22] Y. Wu, H. L. Tepper, and G. A. Voth, J. Chem. Phys. **124**, 024503 (2006).
[23] H. Heinz, H. Koerner, K. L. Anderson, R. A. Vaia, and B. L. Farmer, Chem. Mater. **17**, 5658 (2005).
[24] A. Malani and K. G. Ayappa, J. Phys. Chem. B **113**, 1058 (2009).
[25] R. Saito, R. Matsuo, T. Kimura, G. Dresselhaus, and M. Dresselhaus, Chem. Phys. Lett. **348**, 187 (2001).
[26] P. A. Thompson and M. O. Robbins, Phys. Rev. A **41**, 6830 (1990).
[27] P. A. Thompson and M. O. Robbins, Nature **389**, 360 (1997).
[28] S. Plimpton, J. Comp. Phys. **117**, 1 (1995).
[29] Q. Li, T. E. Tullis, D. Goldsby, and R. W. Carpick, Nature **480**, 233 (2011).
[30] See Supplemental Material at [URL will be inserted by publisher] for density profiles of the graphene-confined system, and for the dependence of friction force on the sliding velocity.
[31] J. Chen, I. Ratera, J. Y. Park, and M. Salmeron, Phys. Rev. Lett. **96**, 236102 (2006).
[32] S. Ohnishi and A. Stewart, Langmuir **18**, 6140 (2002).
[33] E. Riedo, F. Lévy, and H. Brune, Phys. Rev. Lett. **88**, 185505 (2002).
[34] R. Szoszkiewicz and E. Riedo, Phys. Rev. Lett. **95**, 135502 (2005).
[35] G. Cicero, J. C. Grossman, E. Schwegler, F. Gygi, and G. Galli, J. Am. Chem. Soc. **130**, 1871 (2008).
[36] Y. Leng and P. T. Cummings, Phys. Rev. Lett. **94**, 026101 (2005).
[37] R Development Core Team, *R: A Language and Environment for Statistical Computing*, R Foundation for Statistical Computing, Vienna, Austria (2011), ISBN 3-900051-07-0.